

## Compression modes and the nuclear matter incompressibility coefficient

SHALOM SHLOMO

Cyclotron Institute, Texas A&M University, College Station, Texas 77843, USA

**Abstract.** We review the current status of the nuclear matter ( $N = Z$  and no Coulomb interaction) incompressibility coefficient,  $K_{nm}$ , and describe the theoretical and the experimental methods used to determine  $K_{nm}$  from properties of compression modes in nuclei. In particular we consider the long standing problem of the conflicting results obtained for  $K_{nm}$ , deduced from experimental data on excitation cross sections for the isoscalar giant monopole resonance (ISGMR) and data for the isoscalar giant dipole resonance (ISGDR).

**Keywords.** Incompressibility; giant monopole resonance; isoscalar giant monopole resonance.

**PACS Nos** 21.65.+f; 24.30.Cz

### 1. Introduction

Accurate determination of the nuclear matter (NM) equation of state (EOS),  $E = E(\rho)$ , is very important for the study of properties of nuclei, supernova collapse, neutron stars and heavy ion collisions. Only the saturation (minimum) point of the EOS at zero temperature is known with good accuracy. From the NM extrapolation of the empirical mass formula we have  $E(\rho_0) = -16$  MeV and from electron scattering analysis we have  $\rho_0 = 0.17$  fm<sup>-3</sup>. An accurate determination of the NM incompressibility coefficient,  $K_{nm}$ , is needed in order to extend our knowledge of the EOS, since  $K_{nm}$  is directly related to the curvature of the nuclear matter equation of state, [1], at the saturation point ( $E, \rho$ ) = (-16 MeV, 0.17 fm<sup>-3</sup>). The coefficient  $K_{nm}$  is defined by

$$K_{nm} = k_f^2 \frac{d^2(E/A)}{dk_f^2} \Big|_{k_{f0}} = 9\rho_0^2 \frac{d^2(E/A)}{d\rho^2} \Big|_{\rho_0}, \quad (1)$$

where  $E/A$  is the binding energy per particle of the nuclear matter, and  $k_{f0}$  and  $\rho_0$  are the Fermi momentum and the matter density, respectively, at saturation.

There have been quite a few attempts to determine  $K_{nm}$  by considering properties of nuclei which are sensitive to a certain extent to the value of  $K_{nm}$  (see [2]). In a microscopic approach analysis of the experimental data of a certain physical quantity which is sensitive to  $K_{nm}$ , one considers various effective two-body interactions which differ in their value for  $K_{nm}$  but reproduce data of other physical quantities fairly well. One then

determines the effective interaction which best fit the data which is sensitive to  $K_{nm}$ , leading to a constraint on the value of  $K_{nm}$ . In a macroscopic approach analysis,  $K_{nm}$  appears in the expression for the physical quantity under consideration. The value of  $K_{nm}$  is thus deduced by a direct fit to the data. We mention in particular the attempts [2] considering the physical quantities: nuclear masses, nuclear radii, supernova collapses, masses of neutron stars, matter flow in heavy ion collisions and the interaction parameters  $F_0$  and  $F_1$  in Landau's Fermi liquid theory. However, these attempts were not able to determine the value of  $K_{nm}$  to better than a factor of two. Here we examine the most sensitive method [1,3] which is based on experimental data on the strength function distribution of the isoscalar giant monopole resonance (ISGMR),  $L = 0, T = 0$ , and the isoscalar giant dipole resonance (ISGDR),  $L = 1, T = 0$ , which are compression modes of nuclei.

The discovery of the isovector giant dipole resonance (IVGDR),  $L = 1, T = 1$ , by photon excitation over sixty years ago [4] marked the beginning of the experimental and theoretical study of collective motion in nuclei. The discovery of the isoscalar giant quadrupole resonance (ISGQR),  $L = 2, T = 0$ , using inelastic scattering of electron and hadrons [5], led to a significant increase in experimental and theoretical work on the properties of giant resonances in the early 1970's. Around the same time, self-consistent Hartree-Fock (HF) calculations for heavy nuclei became possible with the introduction of Skyrme type interactions [6], which are density and momentum dependent delta interactions. Carrying out self-consistent HF calculations with a Skyrme type interaction, the parameters of the interaction are varied so as to reproduce experimental data of a wide range of nuclei on nuclear masses, nucleon separation energies, charge and mass density distributions, etc. The parameters of the interaction are further constrained by considering experimental data on the nuclear response function (giant resonances). The nuclear response function is evaluated within the (continuum) random-phase-approximation (RPA), i.e., small amplitude oscillation [7]. These earlier Skyrme type interactions [6], which nicely reproduced gross properties of nuclei (such as nuclear mass and radii) and the available data on the IVGDR and the ISGQR, yielded values of about 370 MeV for  $K_{nm}$ . With these interactions, the isoscalar giant monopole resonance (ISGMR) in  $^{208}\text{Pb}$  was predicted to be located at an excitation energy of about 18 MeV.

The discovery of the isoscalar giant monopole resonance (ISGMR) in  $^{208}\text{Pb}$  at excitation energy of 13.7 MeV [8] led to modification of existing effective interactions. Random phase approximation (RPA) calculations using existing or modified effective interactions having  $K_{nm} = 210 \pm 30$  MeV were in agreement with experiment [9]. However, it is worthwhile to note the following: (i) Only a limited class of effective interactions were explored. (ii) For a certain interaction, calculations of the strength distribution of the ISGMR were carried out only for a limited number of nuclei. (iii) Possible effects of more complicated configurations, such as  $2p - 2h$  were ignored.

There have been several attempts [10] in the past to determine  $K_{nm}$  by a least square (LS) fit to the ISGMR data of various sets of nuclei using a semi-empirical expansion of the nucleus incompressibility coefficient,  $K_A$ , in power of  $A^{-1/3}$ . The value deduced for  $K_{nm}$  varied significantly, depending on the set of data of the ISGMR used in the fit. Several things need to be done to pin down  $K_{nm}$ : (i) We need measurements on considerably more than 16 nuclei in which all the energy weighted sum rule (EWSR) has been determined and with more variation in mass. (ii) To the extent possible, spherical nuclei should be chosen to eliminate effects of deformation. (iii) These measurements need to provide the centroid and width of the ISGMR to better than 150 keV. (iv) Significant systematic errors between

differing measurements must be removed. (v) The strength distribution in light nuclei must be mapped over a wide energy range.

Over the last two decades, a significant amount of experimental work was carried out to identify strength distributions of the ISGMR [10] and ISGDR [11] in nuclei. The main experimental tool for studying isoscalar giant resonances is inelastic  $\alpha$ -particle scattering. There are several reasons for this. First,  $\alpha$ -particles are selective as to exciting isoscalar modes which either eliminates or greatly reduces interference of other excitations. Second, angular distributions of inelastically scattered  $\alpha$ -particles at small angles are characteristic for some of the multipolar modes which makes it possible to identify contributions from these excited modes in the experimentally measured angular distributions. The main development in the area of experimental investigation of the isoscalar giant resonances is the high accuracy data obtained at Texas A&M University using a beam analysis system (BAS), a multipole-dipole-multipole (MDM) spectrometer and broad range multiwire proportional counter. The new system improved the signal to background ratio by a factor of 15. This led to the discovery of high lying structure for the ISGMR thereby resolving the discrepancy seen in the mass dependence of the centroid energy between experiment and HF-RPA calculations. Also, more than 50% of the ISGMR EWSR has been located in light nuclei. Moreover, preliminary results [11] for the ISGDR lead to values for its centroid energy which are smaller by 3–5 MeV than those obtained by HF-RPA calculations carried out with effective interactions which reproduce the ISGMR data. Thus, the value of  $K_{nm}$  deduced from the ISGDR data is significantly smaller than that deduced from the ISGMR data.

On the theoretical side, the experimental data pose a challenge to theory [12] to understand the conflicting results for  $K_{nm}$  deduced from the data on the ISGMR and the data on the ISGDR.

We emphasize that it is quite common in theoretical work on giant resonance to calculate the transition strength distribution  $S(E)$  for a certain scattering operator  $F$  whereas in the analysis of experimental data of the excitation cross section  $\sigma(E)$  one carries out distorted-wave-Born-approximation (DWBA) calculations with a certain transition potential. In this work we address the discrepancy between theory and experiment by examining the relation between  $S(E)$  and  $\sigma(E)$  of the ISGMR and the ISGDR, obtained by  $\alpha$ -scattering. For the ISGDR, we also describe and apply an accurate and general method to eliminate the contributions of spurious state mixing from  $S(E)$  and the transition density  $\rho_t(\mathbf{r})$ . We present results of accurate microscopic calculations for  $S(E)$  and for  $\sigma(E)$  with the folding model (FM) DWBA with  $\rho_t(\mathbf{r})$  obtained from HF-RPA calculations. We provide a simple explanation for the discrepancy between theory and experiment concerning the ISGMR and ISGDR.

## 2. Self-consistent HF-RPA approach

In the microscopic and self-consistent Hartree–Fock (HF) random-phase-approximation (RPA) approach one starts by adopting specific effective nucleon–nucleon interaction,  $V_{12}$ , such as the Skyrme type interaction, involving a set of a few parameters. The parameters are varied in the HF calculations so as to reproduce experimental data of a wide range of nuclei on nuclear masses, charge and mass density distributions, nucleon separation energies, etc. The parameters of the interaction are further constrained by considering experimental

data on giant resonances. The properties of the giant resonances are then calculated with the self-consistent HF-RPA approach by solving the RPA equation using the particle-hole (p-h) interaction  $V_{\text{ph}}$  which corresponds to  $V_{12}$ . The RPA Green's function  $G$  [7,13] is obtained from

$$G = G_0(1 + V_{\text{ph}}G_0)^{-1}, \quad (2)$$

where  $G_0$  is the free p-h Green's function. For the scattering operator,

$$F = \sum_{i=1}^A f(\mathbf{r}_i), \quad (3)$$

the strength function is given by

$$S(E) = \sum_n |\langle 0|F|n\rangle|^2 \delta(E - E_n) = \frac{1}{\pi} \text{Im} [\text{Tr}(fGf)], \quad (4)$$

and the corresponding transition density is obtained from

$$\rho_t(\mathbf{r}, E) = \frac{1}{\sqrt{S(E)}} \int f(\mathbf{r}') \left[ \frac{1}{\pi} \text{Im}G(\mathbf{r}', \mathbf{r}, E) \right] d\mathbf{r}'. \quad (5)$$

Note that the definition (5) is consistent with

$$S(E) = \left| \int \rho_t(\mathbf{r}, E) f(\mathbf{r}) d\mathbf{r} \right|^2. \quad (6)$$

In fully self-consistent HF-RPA calculations, the spurious state (associated with the center of mass motion)  $T = 0, L = 1$  appears at zero excitation energy ( $E = 0$ ) and no spurious state mixing (SSM) in the ISGDR occurs. However, although not always stated in the literature, actual implementations of HF-RPA (and relativistic RPA) are not fully self-consistent. One usually makes the following approximations:

- (i) neglecting the two-body Coulomb and spin-orbit interactions in  $V_{\text{ph}}$ ,
- (ii) approximating momentum parts in  $V_{\text{ph}}$ ,
- (iii) limiting the p-h space in a discretized calculation by a cut-off energy  $E_{\text{ph}}^{\text{max}}$ , and
- (iv) introducing a smearing parameter (i.e., a Lorentzian with  $\Gamma/2$ ).

Although the effect of these approximations on the centroid energies of giant resonances is small (less than 1 MeV), the effect on the ISGDR is quite serious since each of these approximations introduces a SSM in the ISGDR.

Recently [14–16], we have shown that in order to correct for the effects of the SSM on  $S(E)$  and the transition density one should replace the scattering operator  $F$ , eq. (3), by the projection operator

$$F_\eta = \sum_{i=1}^A f_\eta(\mathbf{r}_i) = F - \eta F_1, \quad (7)$$

*Compression modes*

with  $f_\eta = f - \eta f_1$ , where  $f(\mathbf{r}) = f(r)Y_{1M}(\Omega)$  and  $f_1(\mathbf{r}) = rY_{1M}(\Omega)$ . The value of  $\eta$  is obtained from the coherent spurious state transition density [17],

$$\rho_{ss}(\mathbf{r}) = \frac{\partial \rho_0}{\partial r} Y_{1M}(\Omega), \quad (8)$$

where  $\rho_0$  is the ground state density of the nucleus, by

$$\eta = \langle f \rho_{ss} \rangle / \langle f_1 \rho_{ss} \rangle. \quad (9)$$

To determine  $\rho_t$  for the ISGDR we first use (5), with  $F_\eta$  and obtain  $\rho_\eta(\mathbf{r})$ . Then we project out the spurious contribution which is proportional to  $\rho_{ss}(\mathbf{r})$ ,

$$\rho_t(\mathbf{r}) = \rho_\eta(\mathbf{r}) - a \rho_{ss}, \quad a = \langle f_1 \rho_\eta \rangle / \langle f_1 \rho_{ss} \rangle. \quad (10)$$

It is important to emphasize that using  $f_\eta$  in (6) with  $\rho_t(\mathbf{r})$  from (10), one obtains the required  $S_\eta(E)$ .

Using the spurious state energy weighted sum rule (EWSR) for the operator  $f_1 = rY_{10}$ , we can write the EWSR of the ISGDR for the scattering operator (3)

$$\sum E_n |\langle 0|F|n\rangle|^2 \delta(E - E_n) = \frac{3}{4\pi} \frac{\hbar^2}{2m} A \left[ \langle 0 | \left( \frac{df}{dr} \right)^2 + 2 \left( \frac{f}{r} \right)^2 | 0 \rangle - \frac{1}{3} \eta^2 \right]. \quad (11)$$

Using (8) and (9), the value of  $\eta$  associated with  $f(\mathbf{r}) = f_3(\mathbf{r}) = r^3 Y_{1M}(\Omega)$ , adopted in our calculations for the ISGDR, is given by

$$\eta = \frac{5}{3} \langle r^2 \rangle. \quad (12)$$

We have carried out numerical calculations for the  $S(E)$ , and  $\rho_t(\mathbf{r})$  within the HF-RPA theory. We used the SL1 Skyrme interaction [18], which is associated with  $K_{nm} = 230$  MeV, and carried out HF calculations using a spherical box of  $R \geq 15$  fm. For the RPA calculations we used the Green's function approach with mesh size  $\Delta r = 0.3$  fm and p-h maximum energy of  $E_{ph}^{max} = 150$  MeV (we include particle states with principle quantum number up to 12), since it is well-known that in order to extract accurate  $\rho_t(\mathbf{r})$ ,  $E_{ph}^{max}$  should be much larger than the value required ( $E_{ph}^{max} \sim 50$  MeV) to recover the EWSR. Since in our calculation we also neglected the two-body Coulomb and spin-orbit interactions, the spurious state energies differ from 0 by a few MeV. We therefore renormalized the strength of the  $V_{ph}$  by a factor, to place the spurious state at  $E = 0.2$  MeV, using the scattering operator  $f = r^3$ . We have included a Lorentzian smearing ( $\Gamma/2 = 1$  MeV) and corrected for the SSM in the ISGDR as described above.

Using the operator  $f = r^2 Y_{00}$  for the ISGMR we calculated the corresponding  $S(E)$ , for  $E$  up to 60 MeV. We recover 100% of the corresponding EWSR. Our HF-RPA results for the ISGMR (E0T0) transition strength distributions in  $^{28}\text{Si}$ ,  $^{40}\text{Ca}$ ,  $^{58}\text{Ni}$ , and  $^{116}\text{Sn}$  nuclei are shown in figure 1. The calculated centroid energies of the ISGMR for  $^{28}\text{Si}$ ,  $^{40}\text{Ca}$ ,  $^{58}\text{Ni}$ ,  $^{116}\text{Sn}$  and  $^{208}\text{Pb}$  nuclei [19,14] are 24.0, 21.1, 21.2, 17.2 and 14.48 MeV, respectively. The corresponding experimental values are  $21.5 \pm 0.3$ ,  $18.9 \pm 0.4$ ,  $20.3 (-0.14)$  ( $+1.69$ ),  $16.07 \pm 0.14$  and  $14.17 \pm 0.28$  MeV, respectively [20].

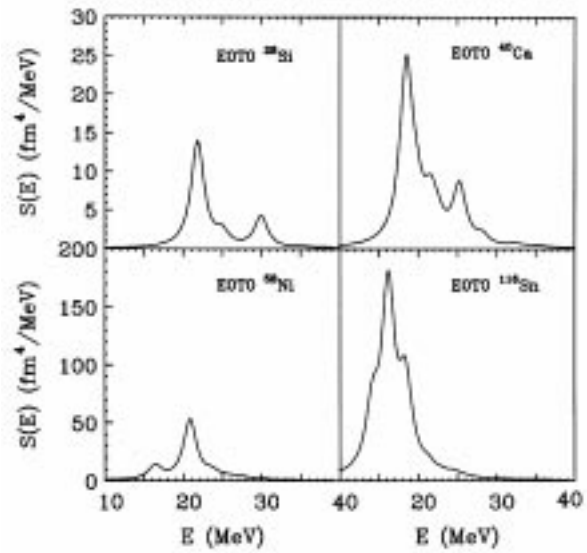


**Figure 1.** Isoscalar monopole strength distributions in  $^{28}\text{Si}$ ,  $^{40}\text{Ca}$ ,  $^{58}\text{Ni}$ , and  $^{116}\text{Sn}$  obtained from the self-consistent HF-RPA calculations.

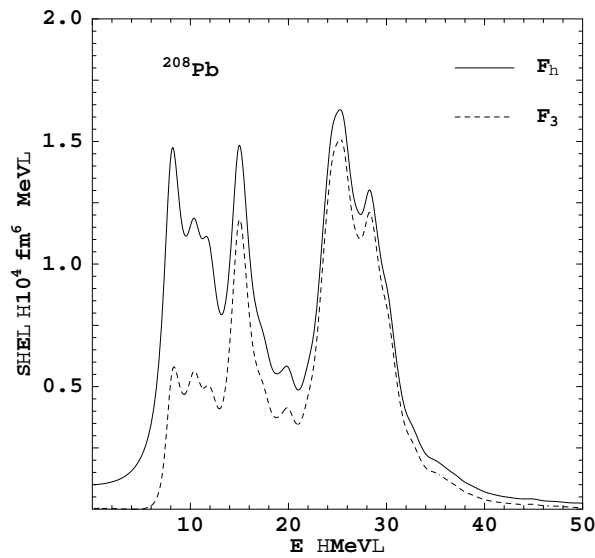


**Figure 2.** Strength functions for the ISGDR in  $^{208}\text{Pb}$  obtained from eqs (5), (10) and (6), using  $f_3$  (dashed line) and  $f_\eta = f_3 - \eta f_1$  (solid line), with  $\eta = 52.1 \text{ fm}^2$ .

Figure 2, exhibits the strength functions for the ISGDR in  $^{208}\text{Pb}$  obtained from eqs (6), (5) and (10). The solid line describes the result obtained using  $f_\eta$ . Note that this result coincides with  $S_\eta(E)$ , which is free of SSM contribution. Similarly, the dashed

line describes the erroneous result obtained using  $f_3$ . We find that when using  $f_3$ , the excitation strengths obtained for certain states are sensitive to the value of  $\Gamma$  [14]. The result obtained with  $f_3$  coincides with that obtained with  $f_\eta$  for  $\Gamma \rightarrow 0$ , as expected. Thus, in the discretized configuration RPA calculation of  $\rho_t$ , one may use  $f_3$  and correct for the SSM contribution before the smearing process.

Our results for the ISGDR,  $S_\eta(E)$ , indicate two main components with the low energy component containing about 20% of the EWSR for  $E$  up to 20, 18 and 16 MeV for  $^{90}\text{Zr}$ ,  $^{116}\text{Sn}$  and  $^{208}\text{Pb}$ , respectively, in agreement with the experimental observation [11]. Similar results were obtained in other calculations [16,14,21,22]. The calculated centroid energies of the higher component ISGDR for  $^{90}\text{Zr}$ ,  $^{116}\text{Sn}$  and  $^{208}\text{Pb}$  nuclei [23] are 31.3, 29.1 and 26.2 MeV, respectively. The corresponding experimental values are  $25.7 \pm 0.7$ ,  $23.0 \pm 0.6$  and  $19.9 \pm 0.8$ , respectively [11].

Our calculations, using the SL1 interaction, reconfirm the well-known result that, at present, HF-RPA calculations for the ISGMR over a wide range of nuclei reproduce the experimental data for effective interactions associated with nuclear matter incompressibility coefficient  $K_{nm} = 210 \pm 30$  MeV. For the ISGDR compression mode we find that the calculated centroid energies are consistently larger than the corresponding experimental values by about 5 MeV. The effective interactions required to reproduce the experimental data for the ISGDR must be associated with a value of  $K_{nm}$  smaller than 170 MeV.

### 3. DWBA calculations of excitation cross section

The distorted wave Born approximation (DWBA) has been widely used in experimental studies in order to give a theoretical description of low-energy scattering reactions and, thus, analyse measured cross sections of scattered probes. The folding model approach [24] to the evaluation of optical potentials appears to be quite successful and is extensively used at present in theoretical descriptions of  $\alpha$ -particle scattering [25]. This approach provides a direct link to the description of  $\alpha$ -particle scattering reactions based on microscopic HF-RPA results.

Within the folding model approach, the optical potential  $U(r)$  is given by

$$U(r) = \int d\mathbf{r}' V(|\mathbf{r} - \mathbf{r}'|, \rho_0(r')) \rho_0(r'), \quad (13)$$

where  $V(|\mathbf{r} - \mathbf{r}'|, \rho_0(r'))$  is the nucleon- $\alpha$  interaction, which is generally complex and density dependent, and  $\rho_0(r')$  is the ground state (Hartree-Fock) density of a spherical target nucleus. It is customary to adopt a certain form for the nucleon- $\alpha$  interaction and obtain the interaction parameters from the fit to experimentally measured elastic angular distributions. In this work, both real and imaginary parts of the nucleon- $\alpha$  interaction are chosen to have the Gaussian shape with density dependence [25]:

$$V(|\mathbf{r} - \mathbf{r}'|, \rho_0(r')) = -V(1 + \beta_V \rho_0^{2/3}(r')) e^{-\frac{|\mathbf{r}-\mathbf{r}'|^2}{\alpha_V}} - iW(1 + \beta_W \rho_0^{2/3}(r')) e^{-\frac{|\mathbf{r}-\mathbf{r}'|^2}{\alpha_W}}. \quad (14)$$

The parameters  $V, \beta_V, \alpha_V$  and  $W, \beta_W, \alpha_W$  in eq. (14) are determined by a fit of the elastic scattering data.

For a state with the multipolarity  $L$  and excitation energy  $E$ , the radial form  $\delta U_L(r, E)$  of the transition potential can be found from

$$\delta U(r, E) = \int d\mathbf{r}' \delta \rho_L(\mathbf{r}', E) \left[ V(|\mathbf{r} - \mathbf{r}'|, \rho_0(r')) + \rho_0(r') \frac{\partial V(|\mathbf{r} - \mathbf{r}'|, \rho_0(r'))}{\partial \rho_0(r')} \right], \quad (15)$$

where  $\delta \rho_L(\mathbf{r}', E)$  is the transition density for the considered state.

At this point, we can distinguish between the microscopic and the macroscopic approaches to the  $\alpha$ -particle scattering description based on the folding model. Within the ‘microscopic’ approach, both the ground state density and the transition density which enter eqs (13) and (15) are obtained from the self-consistent Hartree–Fock–RPA calculations. Within the ‘macroscopic’ approach, the transition densities are assumed to have energy-independent radial shapes and are obtained from the ground state density using the collective model. In particular, the so-called scaling model radial shapes of the transition densities [3] are used in experimental studies of ISGMR ( $L = 0$ ) and ISGDR ( $L = 1$ ) excitations:

$$\delta \rho_{L=0}(r) = -\alpha(E) \left( 3\rho_0(r) + r \frac{d\rho_0(r)}{dr} \right), \quad (16)$$

$$\delta \rho_{L=1}(r) = -\delta_{L=1}(E) \left( 3r^2 \frac{d\rho_0(r)}{dr} + 10r\rho_0(r) - 5/3 \langle r^2 \rangle \frac{d\rho_0(r)}{dr} \right), \quad (17)$$

where the energy-dependent factors  $\alpha(E)$  and  $\delta_{L=1}(E)$  are determined by fitting measured inelastic cross sections. The amounts of E0T0 (ISGMR) or E1T0 (ISGDR) strengths concentrated in a given resonance state can then be deduced from the knowledge of  $\alpha(E)$  and  $\delta_{L=1}(E)$  in a straightforward manner, bearing in mind that for the state  $E_R$  that exhausts 100% of E0T0 or E1T0 EWSR the corresponding coefficient is given by

$$\alpha^2(E_R) = 2\pi \frac{\hbar^2}{mA \langle r^2 \rangle E_R}, \quad (18)$$

$$\delta_{L=1}^2(E_R) = 6\pi \frac{\hbar^2}{mA (11 \langle r^4 \rangle - 25/3 \langle r^2 \rangle^2) E_R}, \quad (19)$$

with  $m$ ,  $A$ , and  $\langle r^K \rangle$  being the nucleon mass, the number of nucleons in the excited nucleus, and the  $K$ th moment of the ground state density, respectively.

It is not clear that the collective model results (16) and (17) are good approximations for the E0T0 and E1T0 transition densities, especially in lighter nuclei. In the following, we test these approximations by performing folding model-DWBA analysis of  $\alpha$ -particle scattering by several nuclei ranging from  $^{28}\text{Si}$  to  $^{116}\text{Sn}$ .

At the next stage of our calculations, using eqs (13), (14) and the Hartree–Fock ground state density, we construct the optical potential and determine the parameters of the

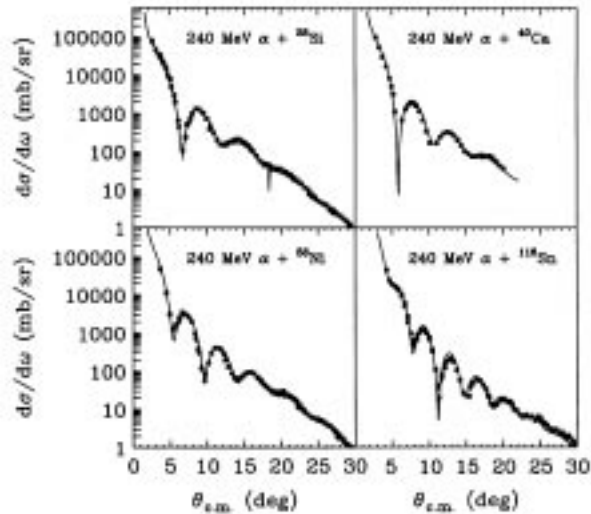


**Figure 3.** Elastic angular distributions for 240 MeV  $\alpha$ -particles. Filled squares represent the experimental data taken from refs [27–30]. Solid lines are our fit to the experimental data using the folding model - DWBA with nucleon- $\alpha$  interaction given in eq. (14).

nucleon- $\alpha$  interaction ( $V_{\alpha n}$ ) of eq. (14) by fitting experimentally measured elastic scattering angular distributions. Numerical DWBA calculations were performed with the computer program PTOLEMY [26]. Quite satisfactory fits, shown in figure 3, were obtained.

Having determined the parameters of the nucleon- $\alpha$  interaction, we calculated the cross sections of inelastically scattered  $\alpha$ -particles for the case of E0T0 and E1T0 excitations of target nuclei using the transition potential (15) and both the RPA transition densities and the collective model transition densities obtained using the Hartree-Fock ground state density and eqs (16) and (17). These transition densities were calculated for each energy value on the 0.2 MeV grid.

In order to see more clearly the impact of radial shape differences between the microscopic and the collective model transition densities on the results of the cross section analysis, we assumed that the cross sections calculated using the RPA transition densities are the actual experimental data to be analysed by performing folding model – DWBA calculations with the collective model shapes of transition densities. In this case the extracted transition strength distributions and centroid energies can be directly compared to the corresponding results of the RPA calculations and discrepancies may occur only as a result of the approximation of transition densities by the collective model shapes.

The procedure for extracting the E0T0 strength from the cross sections is presented in figure 4 for  $^{28}\text{Si}$ . The middle panel of the figure shows  $0^\circ$  double differential E0T0 cross sections obtained with RPA transition density (i.e. our ‘experimental’ data). In the lower panel we show the  $0^\circ$  E0T0 cross sections found using the transition potential (15) with the RPA transition density (solid line) and with the collective model E0T0 transition density (16) (dashed line) normalized to 100% of E0T0 EWSR (see eq. (18)). The dashed

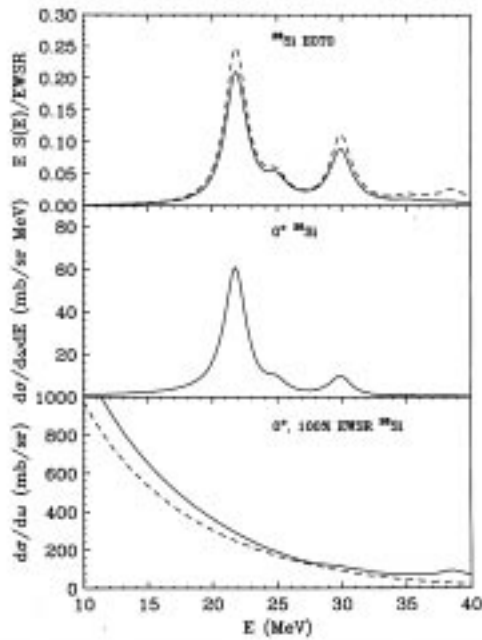


**Figure 4.** Reconstruction of the E0T0 EWSR in  $^{28}\text{Si}$  from the inelastic  $\alpha$ -particle cross sections. The middle panel:  $0^\circ$  double differential E0T0 cross sections obtained with the RPA transition density (i.e. our 'experimental' data). The lower panel:  $0^\circ$  E0T0 cross sections found using the collective model E0T0 transition density (dashed line) and the RPA transition density (solid line), normalized to 100% of the E0T0 EWSR. The upper panel: ratio of the curve in the middle panel and the dashed curve in the lower panel (dashed line), ratio of the curve in the middle panel and the solid curve in the lower panel (solid line). Dashed line in the upper panel represents the fraction of the E0T0 EWSR per unit energy reconstructed from our 'experimental' cross sections while the solid line in the upper panel shows the actual fraction of the E0T0 EWSR per unit energy as calculated using the RPA.

line in the upper panel of the figure is the ratio of the curve in the middle panel and the one in the lower panel. It represents the fraction of the E0T0 EWSR per unit energy reconstructed from our 'experimental' cross sections. The solid line in the upper panel shows the actual fraction of the E0T0 EWSR per unit energy as calculated from the E0T0 transition strength distribution of figure 1. The reconstructed and actual E0T0 EWSR for  $^{40}\text{Ca}$ ,  $^{58}\text{Ni}$  and  $^{116}\text{Sn}$  are shown in figure 5. It can be seen that the cross section analysis based on using the collective model shapes for transition densities tends to overestimate the ISGMR (E0T0) EWSR by up to 20%. Difference in shapes between the collective model and the microscopic transition densities can also lead to deviations of the ISGMR centroid energies deduced from the reconstructed strength distributions from the actual centroid

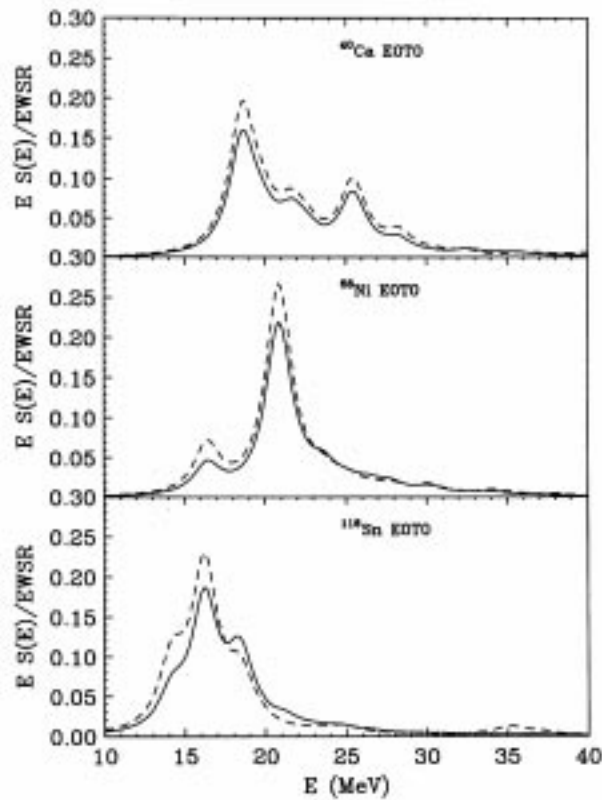


**Figure 5.** Same as the upper panel of figure 4 for  $^{40}\text{Ca}$ ,  $^{58}\text{Ni}$ , and  $^{116}\text{Sn}$ .

energies obtained from microscopic calculations. These shifts, however, are of the order of a few percent and not very significant for the considered nuclei.

Similar analysis was carried out for the excitation cross section of the ISGDR. In figure 6 we present results of microscopic calculations of the excitation cross section of the ISGDR in  $^{116}\text{Sn}$  by 240 MeV  $\alpha$ -particle, carried out within the FM-DWBA. The dashed lines are obtained using  $\rho_{\text{coll}}(r)$  of the ISGDR, eq. (17). It is seen from the upper panel that the use of  $\rho_{\text{coll}}$  increases the EWSR by at least 10% and may shift the centroid energy by a few percent. However, reported experimental values for the fraction of the EWSR are larger than the corresponding calculated values by a factor of 3. An important result of our calculation is that the maximum cross section for the ISGDR drops below the current experimental sensitivity of 2–3 mb/sr/MeV for excitation energy above 32 and 27 MeV, for  $^{116}\text{Sn}$  and  $^{208}\text{Pb}$ , respectively. This high excitation energy region contains about 30% of the EWSR. This missing strength leads to a reduction of more than 3.0 MeV in the ISGDR energy and thus explains the discrepancy between theory and experiment. More sensitive experiments and/or with higher  $\alpha$ -particle energy are thus needed.

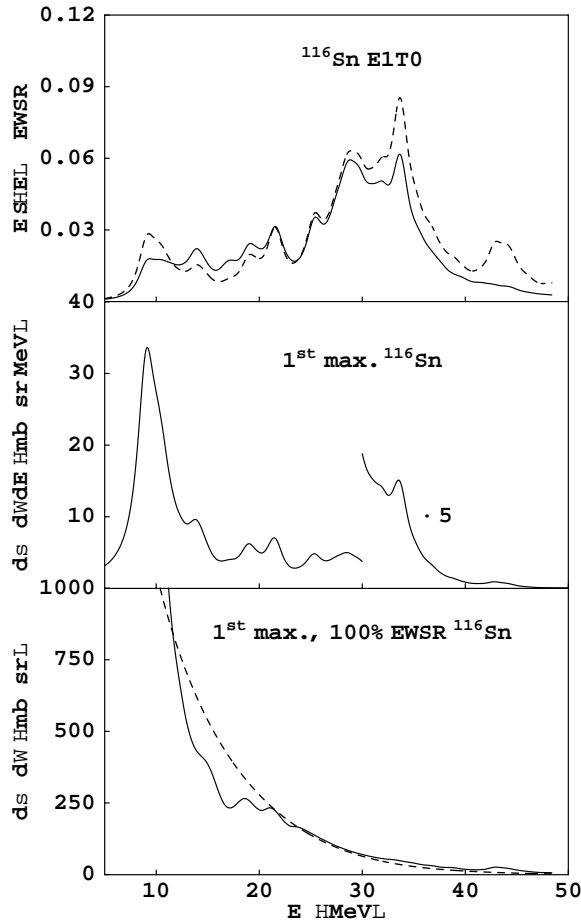


**Figure 6.** Reconstruction of the ISGDR EWSR in  $^{116}\text{Sn}$  from the inelastic  $\alpha$ -particle cross sections (see figure 4). The middle panel: maximum double differential cross section obtained from  $\rho_t$  (RPA). The lower panel: maximum cross section obtained with  $\rho_{\text{coll}}$  (dashed line) and  $\rho_t$  (solid line) normalized to 100% of the EWSR. Upper panel: The solid and dashed lines are the ratios of the middle panel curve with the solid and dashed lines of the lower panel, respectively.

#### 4. Conclusions

We presented results of microscopic calculations of the strength function,  $S(E)$ , within the HF-RPA approach, and  $\alpha$ -particle excitation cross sections  $\sigma(E)$ , using the folding model DWBA, for the isoscalar giant monopole resonance (ISGMR) and the isoscalar giant dipole resonance (ISGDR). An accurate and a general method to eliminate the contributions of spurious state mixing in the ISGDR was used in the calculations. Our results indicate:

For the ISGMR:

- (i) Current experimental methods adopted to extract the strength distribution, which are based on using the collective model shapes for transition densities, tend to overestimate the ISGMR EWSR by up to 20%. However, the resulting shifts in the centroid energies are small, of the order of a few per cent.
- (ii) We reconfirmed the well-known results that effective nucleon–nucleon interactions reproducing the experimental data on the ISGMR are associated with a nuclear matter incompressibility coefficient  $K_{nm} = 210 \pm 30$  MeV.

For the ISGDR:

- (i) Current experimental methods adopted to extract the strength distribution, using the collective model shapes for transition densities, tend to overestimate the ISGDR EWSR by up to 20%. However, the resulting shifts in the centroid energies are small, of the order of a few per cent.
- (ii) Our results for the transition strength distribution, indicate two main components for the ISGDR, with the low energy component containing close to 20% of the EWSR, in agreement with (corrected) recent experimental results.
- (iii) We also find that the calculated centroid energies of the ISGDR compression mode (higher component) are consistently larger than the corresponding experimental values by about 5 MeV. Thus the effective interactions required to reproduce the experimental data for the ISGDR must be associated with a value of  $K_{nm}$  smaller than 170 MeV.
- (iv) An important result of our calculation is that the maximum cross section for the ISGDR drops below the current experimental sensitivity of 2–3 mb/sr/MeV for excitation energy above 32 and 27 MeV for  $^{116}\text{Sn}$  and  $^{208}\text{Pb}$ , respectively. This high excitation energy region contains about 30% of the EWSR. This missing experimental strength leads to a reduction of more than 3.0 MeV in the ISGDR centroid energy and thus explains the discrepancy between theory and experiment. More sensitive experiments and/or with higher  $\alpha$ -particle energy are thus needed.

In order to determine  $K_{nm}$  with accuracy better than 10%, more experimental work is needed to establish the strength distribution of:

- (i) The ISGDR over a wide range of nuclei.
- (ii) The ISGMR for medium, light nuclei and neutron rich nuclei.

Further theoretical investigations are also needed to:

- (i) Carry out analysis of the experimental data on the nuclear response functions, using ground state density and transition densities obtained from microscopic, self-consistent HF-RPA calculations.
- (ii) Obtain good assessment of the effects of more complicated configurations, such as  $2p - 2h$ , on the nuclear response function.

## Acknowledgement

I thank Dr. A I Sanzhur for help in the calculations. This work was supported in part by the US Department of Energy under grant no. DOE-FG03-93ER40773.

## References

- [1] A Bohr and B M Mottelson, *Nuclear structure II* (Benjamin, New York, 1975)
- [2] N K Glendenning, *Phys. Rev.* **C37**, 2733 (1988)
- [3] S Stringari, *Phys. Lett.* **B108**, 232 (1982)
- [4] G C Baldwin and G S Klaiber, *Phys. Rev.* **71**, 3 (1947)
- [5] A Pitthan and Th Walcher, *Phys. Lett.* **318**, 563 (1971)  
M B Lewis and F E Bertrand, *Nucl. Phys.* **A196**, 337 (1972)
- [6] D Vautherin and D M Brink, *Phys. Rev.* **C5**, 626 (1972)  
M Beiner *et al*, *Nucl. Phys.* **A238**, 29 (1975)
- [7] S Shlomo and G Bertsch, *Nucl. Phys.* **A243**, 507 (1975)
- [8] N Marty *et al*, *Nucl. Phys.* **A230**, 93 (1975)  
M N Harakeh *et al*, *Phys. Rev. Lett.* **38**, 676 (1977)  
D H Youngblood *et al*, *Phys. Rev. Lett.* **39**, 1188 (1977)
- [9] J P Blaizot, *Phys. Rep.* **64**, 171 (1980)
- [10] S Shlomo and D H Youngblood, *Phys. Rev.*, **C47**, 529 (1993); and references therein
- [11] H L Clark, Y-W Lui and D H Youngblood, *Phys. Rev.* **63**, 03130 (2001), and references therein
- [12] T S Dumitrescu, and F E Serr, *Phys. Rev.* **C27**, 811 (1983)
- [13] G F Bertsch and S F Tsai, *Phys. Rep.* **18**, 125 (1975)
- [14] S Shlomo and A I Sanzhur, submitted for publication
- [15] M L Gorelik, S Shlomo and M H Urin, *Phys. Rev.* **C62**, 044301 (2000)
- [16] A Kolomiets, O Pochivalov and S Shlomo, *Progress in Research* (Cyclotron Institute, Texas A&M University) April 1, 1998–March 31, 1999, III-1 (1999)
- [17] G F Bertsch, *Suppl. Prog. Theor. Phys.* **74**, 115 (1983)
- [18] K-F Liu, H-D Lou, Z-Y Ma and Q-B Shen, *Nucl. Phys.* **A534**, 1 (1991); **A534**, 25 (1991)
- [19] A Kolomiets, O Pochivalov and S Shlomo, *Phys. Rev.* **C61**, 034312 (2000)
- [20] D H Youngblood, H L Clark and Y-W Lui, *Phys. Rev. Lett.* **82**, 691 (1999)
- [21] G Colo, N VanGiai, P F Bortignon and M R Quaglia *Phys. Lett.* **B485**, 362 (2000)
- [22] D Vretenar, A Wandelt, and P Ring *Phys. Lett.* **B487**, 334 (2000)
- [23] S Shlomo *et al*, to be published
- [24] G R Satchler, *Direct nuclear reactions* (Oxford University Press, Oxford, 1983)
- [25] G R Satchler and D T Khoa, *Phys. Rev.* **C55**, 285 (1997)
- [26] M Rhoades-Brown *et al*, *Phys. Rev.* **C21**, 2417 (1980)  
M H Macfarlane and S C Pieper, Argonne National Laboratory Report No. ANL-76-11, Rev. 1, 1978 (unpublished)
- [27] D H Youngblood, H L Clark and Y-W Lui, *Phys. Rev. Lett.* **76**, 1429 (1996)
- [28] D H Youngblood, Y-W Lui, and H L Clark, *Phys. Rev.* **C55**, 2811 (1997)
- [29] D H Youngblood, H L Clark and Y-W Lui, *Phys. Rev.* **C57**, 1134 (1998)
- [30] H L Clark, Y-W Lui and D H Youngblood, *Phys. Rev.* **C57**, 2887 (1998)